 SID, vol.1, no.2, pp.131-143, 2005

The MLPG Method for Crack Analysis in Anisotropic Functionally Graded Materials

J. Sladek[1], **V. Sladek, Ch.Zhang**[2]

Abstract: A meshless method based on the local Petrov-Galerkin approach is proposed for crack analysis in two-dimensional (2-d), anisotropic and linear elastic solids with continuously varying material properties. Both quasi-static and transient elastodynamic problems are considered. For time-dependent problems, the Laplace-transform technique is utilized. A unit step function is used as the test function in the local weak-form. It is leading to local boundary integral equations (LBIEs) involving only a domain-integral in the case of transient dynamic problems. The analyzed domain is divided into small subdomains with a circular shape. The moving least-squares (MLS) method is adopted for approximating the physical quantities in the LBIEs. The accuracy of the present method for computing the mode-I stress intensity factors is discussed by comparison with available analytical or numerical solutions.

keyword: Anisotropic elasticity, meshless local Petrov-Galerkin method (MLPG), moving least-squares interpolation, Laplace-transform, functionally graded materials (FGMs), Stehfest's inversion, stress intensity factors

1 Introduction

Functionally graded materials (FGMs) possess continuously nonhomogeneous material properties. These materials have been introduced in recent years to benefit from the ideal performance of its constituents, e.g. high heat and corrosion resistance of ceramics on one side, and large mechanical strength and toughness of metals on the other side. In FGMs, the composition and the volume fraction of their constituents vary continuously with spatial coordinates. A review on various aspects of FGMs can be found in the monograph of Suresh and Mortensen (1998) and the review chapter by Paulino et al. (2003). FGMs may exhibit isotropic or anisotropic material properties depending on the processing technique and the practical engineering requirements. In the present paper, anisotropic material properties of FGMs are considered as in many previous papers isotropic FGMs have been investigated, see e.g., [Erdogan (1995); Sladek et al. (2000); Rao and Rahman (2003); Kim and Paulino (2002, 2003)].

The solution of the boundary or initial boundary value problems for continuously nonhomogeneous solids requires advanced numerical methods due to the high mathematical complexity. Beside the well established finite element method (FEM), the boundary element method (BEM) provides an efficient and popular alternative to the FEM for solving certain class of boundary or initial boundary value problems. The conventional BEM is accurate and efficient for many engineering problems. However, it requires to know the fundamental solutions or the Green's functions. The material anisotropy increases the number of elastic constants in Hooke's law, and hence makes the construction of fundamental solutions cumbersome. For 2-d elastostatic problems in homogeneous, anisotropic and linear elastic solids the fundamental solution is available in closed forms [Eshelby et al. (1953); Schclar (1994)] and it is given in a complex variable space. Closed form elastostatic fundamental solutions for 3-d anisotropic elasticity exist only for special cases like transversally isotropic or cubic materials [Ding et al. (1997)]. In contrast to the static case, very few applications of the BEM to elastodynamic problems in homogeneous, anisotropic and linear elastic solids can be found in literature [Wang and Achenbach (1996); Albuquerque et al. (2002a,b); Kögl and Gaul (2000)], although the BEM has been successfully applied to elastodynamic problems in homogeneous, isotropic and linear elastic solids for many years. The main reason lies in the elastodynamic fundamental solutions for anisotropic and linear elastic solids, which cannot be given in simple

[1] Institute of Construction and Architecture, Slovak Academy of Sciences, 84503 Bratislava, Slovakia, email: sladek@savba.sk

[2] Department of Civil Engineering, University of Siegen, D-57068 Siegen, Germany, email: c.zhang@uni-siegen.de

and closed forms and thus make their numerical implementation somewhat cumbersome. Time-domain elastodynamic fundamental solutions for 2-d anisotropic and linear elastic solids have been applied by Wang et al. (1996) to transient wave scattering analysis by a cavity. The dual reciprocity BEM has been used by Albuquerque et al. (2002a,b) and Kögl and Gaul (2000), where the corresponding elastostatic fundamental solutions have been utilized.

The fracture and the fatigue properties of ceramic/metal FGMs are important to their mechanical integrity, reliability and durability [Paulino et al. (2003a)] in practical engineering applications. The microstructure of FGMs is generally heterogeneous, and the dominant type of failure in ceramic/metal FGMs is crack initiation and growth from inclusions. The influence of material properties especially the composition and the microstructure on crack-driving forces in FGMs is still not well understood. Such issues have motivated much of the current research works on numerical simulations to gain a better understanding of the fracture processes in FGMs. The asymptotic crack-tip stress and displacement fields have the same form as those in homogeneous materials. The effect of the material property variation manifests itself in the near tip stress intensity factors as well as the higher order terms in the asymptotic expansion [Kim and Paulino (2002, 2003a,b), Dolbow and Gosz (2002)]. Due to the high mathematical complexity of the boundary or initial-boundary value problem, most investigations on cracked FGMs known in literature were restricted to isotropic materials. Gu and Asaro (1997) studied orthotropic FGMs considering a four-point bending specimen with varying Young's modulus and varying Poisson‘s ratio. Ozturk and Erdogan (1997, 1999) used the singular integral equation method to investigate mode-I and mixed-mode crack problems in an infinite nonhomogeneous orthotropic medium with a crack aligned to one of the principal material axes and a constant Poisson‘s ratio. Kim and Paulino (2003b, 2004) computed stress intensity factors and T-stresses in orthotropic FGMs using the FEM and interaction integral method.

In this paper a new computational method is developed to analyze boundary value problems in anisotropic FGMs with cracks. The governing equations for nonhomogeneous, anisotropic and linear elastic solids are more complex than that for the homogeneous counterpart. The material nonhomogeneity gives rise to an additional complication in the derivation of elastostatic and elastodynamic fundamental solutions. For general nonhomogeneous, anisotropic and linear elastic solids, elastostatic and elastodynamic fundamental solutions are yet, to the best of the authors knowledge, still not available. One possibility to obtain a BEM formulation is based on the use of fundamental solutions for a fictitious homogeneous medium [Sladek et al. (1993)]. This approach, however, leads to a boundary-domain integral formulation with a domain-integral containing the gradients of the primary fields. The boundary-domain formulation, however, brings some computational difficulties in the numerical implementation. To overcome this difficulty a local integral formulation can be used for general nonhomogeneous solids [Sladek et al. (2000); Mikhailov (2002)]. The application of local integral equations (LIEs) requires the use of a domain approximation of the physical fields in the numerical implementation. In recent years, meshless formulations are becoming popular due to their higher adaptivity and lower cost for preparing input data in the numerical analysis. Several meshless methods haven been proposed so far in literature [Belytschko et al. (1994); Atluri and Shen (2002); Atluri (2004)]. Many of them are derived from a weak-form formulation on global domain or a set of local subdomains. The global formulation requires background cells for the integration of the weak-form. In contrast, the local weak-form formulation needs no cells and therefore the corresponding methods are often called truly meshless methods. If a simple form for the geometry of the subdomains is chosen, numerical integrations over them can be easily carried out. The meshless local Petrov-Galerkin (MLPG) method is a fundamental base for the derivation of many meshless formulations, since trial and test functions can be chosen from different functional spaces. If a unit step function is used as the test function in the local weak-form to derive LIEs, the form of LIEs is much simpler than that provided by utilizing the singular fundamental solutions. Such an approach has been recently applied to problems in homogeneous, anisotropic and linear elastic solids by Sladek et al. (2004). In this paper that approach is extended to continuously nonhomogeneous, anisotropic and linear elastic solids. It yields a pure contour or boundary integral formulation on local boundaries for static problems in anisotropic linear elasticity. In anisotropic elastodynamics an additional domain-integral containing the in-

ertial terms is involved. The Laplace-transform is applied to eliminate the time variable in the governing equations and the boundary conditions of elastodynamic problems. Then, the local boundary integral equations are derived in the Laplace-transformed domain. Several quasi-static boundary value problems have to be solved for various values of the Laplace-transform parameter. The integral equations have a very simple nonsingular form. Moreover, both the contour and domain integrations can be easily carried out on circular subdomains. The Stehfest's inversion method [Stehfest (1970)] is applied to obtain the time-dependent solutions. The spatial variation of the displacements is approximated by the moving least-squares (MLS) scheme. Several numerical examples for crack problems in nonhomogeneous anisotropic and linear elastic solids are presented and discussed.

2 Basic equations of crack analysis in anisotropic FGMs

Let us consider a linear elastodynamic problem in an anisotropic continuously nonhomogeneous and linear elastic domain Ω bounded by the boundary Γ. The equilibrium equations can be expressed as

$$\sigma_{ij,j}(\boldsymbol{x},t)-\rho(\boldsymbol{x})\ddot{u}_i(\boldsymbol{x},t)=-X_i(\boldsymbol{x},t), \tag{1}$$

where $\sigma_{ij}(\boldsymbol{x},t)$ is the stress tensor, $X_i(\boldsymbol{x},t)$ is the body force vector, $\rho(x)$ is the mass density, $u_i(\boldsymbol{x},t)$ is the displacement vector, and the dots indicate the second time derivative. A comma denotes partial differentiation with respect to the spatial coordinates. An elastostatic problem can be considered formally as a special case of the elastodynamic one by omitting the acceleration $\ddot{u}_i(\boldsymbol{x},t)$ in the equilibrium equations (1). Therefore, both cases are analyzed simultaneously.

In the case of linear elastic materials, the relation between the stresses and strains are given by Hooke's law

$$\sigma_{ij}(\boldsymbol{x},t)=C_{ijkl}(\boldsymbol{x})\varepsilon_{kl}(\boldsymbol{x},t)=C_{ijkl}(\boldsymbol{x})u_{k,l}(\boldsymbol{x},t), \tag{2}$$

where $C_{ijkl}$is the elasticity tensor which exhibits the symmetries

$$C_{ijkl}=C_{jikl}=C_{klij}.$$

The traction vector $t_i(\boldsymbol{x},t)$ is related to the displacement vector through Cauchy's formula $t_i=\sigma_{ij}n_j$, which leads to

$$t_i(\boldsymbol{x},t)=C_{ijkl}(\boldsymbol{x})u_{k,l}(\boldsymbol{x},t)n_j(\boldsymbol{x}), \tag{3}$$

where n_j denotes an outward unit normal vector.

For a plane stress state of a 2-d anisotropic and linear elastic solid, the generalized Hooke's law is frequently represented by the second order tensor of the elastic constants [Lekhnitskii (1963)]

$$\begin{bmatrix}\varepsilon_{11}\\ \varepsilon_{22}\\ \gamma_{12}\end{bmatrix}=\begin{bmatrix}\beta_{11}&\beta_{12}&\beta_{16}\\ \beta_{12}&\beta_{22}&\beta_{26}\\ \beta_{16}&\beta_{26}&\beta_{66}\end{bmatrix}\begin{bmatrix}\sigma_{11}\\ \sigma_{22}\\ \sigma_{12}\end{bmatrix}, \tag{4}$$

where β_{ij} are the elastic compliance coefficients of the material. In the case of a plane strain condition, the coefficients β_{ij}should be replaced by $\tilde{\beta}_{ij}$, where

$$\tilde{\beta}_{ij}=\beta_{ij}-\frac{\beta_{i3}\beta_{j3}}{\beta_{33}}.$$

The compliance coefficients can be expressed in terms of engineering constants as

$$\begin{aligned}
&\beta_{11}=1/E_1,\\
&\beta_{22}=1/E_2,\\
&\beta_{12}=-\nu_{12}/E_1=-\nu_{21}/E_2,\\
&\beta_{16}=\eta_{12,1}/E_1=\eta_{1,12}/G_{12},\\
&\beta_{26}=\eta_{12,2}/E_2=\eta_{2,12}/G_{12},\\
&\beta_{66}=1/G_{12}
\end{aligned} \tag{5}$$

where E_k are the Young's moduli refering to the axes x_k, G_{12} is the shear modulus for the in-plane, ν_{ij} are Poisson's ratios, and $\eta_{jk,l}$ and $\eta_{l,jk}$ are the mutual coefficients of first and second kind, respectively. For orthotropic materials $\beta_{16}=\beta_{26}=0$. For plane stress problem in orthotropic materials the stress-strain relation can be written as

$$\begin{bmatrix}\sigma_{11}\\ \sigma_{22}\\ \sigma_{12}\end{bmatrix}=\mathbf{D}(\boldsymbol{x})\begin{bmatrix}\varepsilon_{11}\\ \varepsilon_{22}\\ 2\varepsilon_{12}\end{bmatrix}, \tag{6}$$

where

$$\mathbf{D}(\boldsymbol{x})=\begin{bmatrix}E_1/e&E_2\nu_{12}/e&0\\ E_2\nu_{12}/e&E_2/e&0\\ 0&0&G_{12}\end{bmatrix}$$

with $e=1-\frac{E_2}{E_1}(\nu_{12})^2$. The following boundary and initial conditions are assumed

$u_i(\boldsymbol{x},t)=\tilde{u}_i(\boldsymbol{x},t),\quad$ on Γ_u,

$t_i(\boldsymbol{x},t)=\tilde{t}_i(\boldsymbol{x},t), \quad$ on Γ_t,

$u_i(\boldsymbol{x},t)|_{t=0}=u_i(x,0)$ and $\dot{u}_i(\boldsymbol{x},t)|_{t=0}=\dot{u}_i(x,0)$ in Ω,

where Γ_u is the part of the global boundary with prescribed displacements and on Γ_t the traction vector is given.

The structure of the stress and the displacement fields in a small vicinity of the crack-tip in continuously nonhomogeneous medium is the same as in a homogeneous one. For a mode-I crack the crack-tip stress and displacement fields are given by [Sih et al. (1965)]

$$
\begin{aligned}
\sigma_{11} &= \frac{K_I}{\sqrt{2\pi r}} Re\left[\frac{\mu_1^{\text{tip}}\mu_2^{\text{tip}}}{\mu_1^{\text{tip}}-\mu_2^{\text{tip}}}\right. \\
&\left.\left(\frac{\mu_2^{\text{tip}}}{\sqrt{\cos\theta+\mu_2^{\text{tip}}\sin\theta}}-\frac{\mu_1^{\text{tip}}}{\sqrt{\cos\theta+\mu_1^{\text{tip}}\sin\theta}}\right)\right], \\
\sigma_{22} &= \frac{K_I}{\sqrt{2\pi r}} Re\left[\frac{1}{\mu_1^{\text{tip}}-\mu_2^{\text{tip}}}\right. \\
&\left.\left(\frac{\mu_1^{\text{tip}}}{\sqrt{\cos\theta+\mu_2^{\text{tip}}\sin\theta}}-\frac{\mu_2^{\text{tip}}}{\sqrt{\cos\theta+\mu_1^{\text{tip}}\sin\theta}}\right)\right], \\
\sigma_{12} &= \frac{K_I}{\sqrt{2\pi r}} Re\left[\frac{\mu_1^{\text{tip}}\mu_2^{\text{tip}}}{\mu_1^{\text{tip}}-\mu_2^{\text{tip}}}\right. \\
&\left.\left(\frac{1}{\sqrt{\cos\theta+\mu_1^{\text{tip}}\sin\theta}}-\frac{1}{\sqrt{\cos\theta+\mu_2^{\text{tip}}\sin\theta}}\right)\right], \\
u_1 &= K_I\sqrt{\frac{2r}{\pi}} Re\left[\frac{1}{\mu_1^{\text{tip}}-\mu_2^{\text{tip}}}\right. \\
&\left.\left(\mu_1^{\text{tip}}P_{12}\sqrt{\cos\theta+\mu_2^{\text{tip}}\sin\theta}-\mu_2^{\text{tip}}P_{11}\sqrt{\cos\theta+\mu_1^{\text{tip}}\sin\theta}\right)\right] \\
u_2 &= K_I\sqrt{\frac{2r}{\pi}} Re\left[\frac{1}{\mu_1^{\text{tip}}-\mu_2^{\text{tip}}}\right. \\
&\left.\left(\mu_1^{\text{tip}}P_{22}\sqrt{\cos\theta+\mu_2^{\text{tip}}\sin\theta}-\mu_2^{\text{tip}}P_{21}\sqrt{\cos\theta+\mu_1^{\text{tip}}\sin\theta}\right)\right]
\end{aligned}
\tag{7}
$$

where **Re** denotes the real part of a complex function, μ_i^{tip} are material parameters at the crack-tip, which are roots of the following characteristic equation [Lekhnitskii (1963)]

$$\beta_{11}\mu^4-2\beta_{16}\mu^3+(2\beta_{12}+\beta_{66})\mu^2-2\beta_{26}\mu+\beta_{22}=0, \tag{8}$$

and

$$P_{ik}=\begin{bmatrix}\beta_{11}\mu_k^2+\beta_{12}-\beta_{16}\mu_k\\ \beta_{12}\mu_k+\beta_{22}/\mu_k-\beta_{26}\end{bmatrix}. \tag{9}$$

In Eq. (7), polar coordinate system with the origin at the crack-tip is used.

3 Local boundary integral equations in Laplace-transformed domain

Applying the Laplace-transform to the governing equations (1), we have

$$\overline{\sigma}_{ij,j}(\boldsymbol{x},p)-\rho(\boldsymbol{x})p^2\overline{u}_i(\boldsymbol{x},p)=-\overline{F}_i(\boldsymbol{x},p), \tag{10}$$

where

$$\overline{F}_i(\boldsymbol{x},p)=\overline{X}_i(\boldsymbol{x},p)+pu_i(\boldsymbol{x},0)+\dot{u}_i(\boldsymbol{x},0)$$

is the redefined body force in the Laplace-transformed domain with the initial boundary conditions for displacements $u_i(\boldsymbol{x},0)$ and velocities $\dot{u}_i(\boldsymbol{x},0)$.

The Laplace-transform of a function $f(\boldsymbol{x},t)$ is defined as

$$L[f(x,t)]=\overline{f}(x,p)=\int_0^\infty f(\boldsymbol{x},t)e^{-pt}d\tau,$$

where p is the Laplace-transform parameter.

Instead of writing the global weak-form for the above governing equations, the MLPG methods construct the weak-form over local subdomains such as Ω_s, which is a small region taken for each node inside the global domain [Atluri and Shen (2002)]. The local subdomains overlap each other, and cover the whole global domain Ω. The local subdomains could be of any geometric shape and size. In the present paper, the local subdomains are taken to be of a circular shape. The local weak-form of the governing equations (10) can be written as

$$\int_{\Omega_s}\left[\overline{\sigma}_{ij,j}(\boldsymbol{x},p)-\rho(x)p^2\overline{u}_i(\boldsymbol{x},p)+\overline{F}_i(\boldsymbol{x},p)\right]u_i^*(\boldsymbol{x})d\Omega=0, \tag{11}$$

where $u_i^*(\boldsymbol{x})$ is a test function.

Using

$$\sigma_{ij,j}u_i^*=\left(\sigma_{ij}u_i^*\right)_{,j}-\sigma_{ij}u_{i,j}^*$$

and applying the Gaussian divergence theorem one can write

$$\int_{\partial\Omega_s} \overline{\sigma}_{ij}(\boldsymbol{x},p)n_j(\boldsymbol{x})u_i^*(\boldsymbol{x})d\Gamma - \int_{\Omega_s} \overline{\sigma}_{ij}(\boldsymbol{x},p)u_{i,j}^*(\boldsymbol{x})d\Omega + \int_{\Omega_s} \left[-\rho(x)p^2\overline{u}_i(\boldsymbol{x},p)+\overline{F}_i(\boldsymbol{x},p)\right]u_i^*(\boldsymbol{x})d\Omega = 0, \tag{12}$$

where $\partial\Omega_s$ is the boundary of the local subdomain which consists of three parts $\partial\Omega_s = L_s \cup \Gamma_{st} \cup \Gamma_{su}$. Here, L_s is the local boundary that is totally inside the global domain, Γ_{st} is the part of the local boundary which coincides with the global traction boundary, i.e., $\Gamma_{st} = \partial\Omega_s \cap \Gamma_t$, and similarly Γ_{su} is the part of the local boundary that coincides with the global displacement boundary, i.e., $\Gamma_{su} = \partial\Omega_s \cap \Gamma_u$ (see Fig. 1).

If a unit step function is chosen as the test function $u_i^*(\boldsymbol{x})$ in each subdomain

$$u_i^*(\boldsymbol{x}) = \begin{cases} 1 \text{ at } \boldsymbol{x} \in \Omega_s \\ 0 \text{ at } \boldsymbol{x} \notin \Omega_s \end{cases}$$

and considering

$$\overline{t}_i(\boldsymbol{x},p) = \overline{\sigma}_{ij}(\boldsymbol{x},p)n_j(\boldsymbol{x})$$

the local weak-form (12) is leading to local boundary integral equations

$$\int_{\partial\Omega_s} \overline{t}_i(\boldsymbol{x},p)d\Gamma + \int_{\Omega_s} \left[-\rho(x)p^2\overline{u}_i(\boldsymbol{x},p)+\overline{F}_i(\boldsymbol{x},p)\right]d\Omega = 0. \tag{13}$$

Rearranging unknown terms on the left-hand side we get

$$\int_{L_s} \overline{t}_i(\boldsymbol{x},p)d\Gamma + \int_{\Gamma_{su}} \overline{t}_i(\boldsymbol{x},p)d\Gamma - \int_{\Omega_s} \rho(x)p^2\overline{u}_i(\boldsymbol{x},p)d\Omega = -\int_{\Gamma_{st}} \bar{\overline{t}}_i(\boldsymbol{x},p)d\Gamma - \int_{\Omega_s} \overline{F}_i(\boldsymbol{x},p)d\Omega. \tag{14}$$

Equation (14) is recognized as the overall force equilibrium equation on the subdomain Ω_s. In the case of static problems the domain-integral on the left-hand side of this local boundary integral equation disappears. Then, a pure contour-integral formulation is obtained under the assumption of vanishing body forces and zero initial conditions.

In the MLPG method the test and the trial functions are not necessarily from the same functional spaces. For internal nodes, the test function is chosen as a unit step function with its support on the local subdomain. The trial function, on the other hand, is chosen to be the moving least-squares (MLS) interpolation over a number of nodes randomly spread within the domain of influence. While the local subdomain is defined as the support of the test function on which the integration is carried out, the domain of influence is defined as a region where the weight function is not zero and all nodes lying inside are taken for the interpolation. The approximated function can be written as [Atluri and Shen (2002)]

$$\overline{\boldsymbol{u}}^h(\boldsymbol{x},p) = \boldsymbol{\Phi}^T(\boldsymbol{x}) \cdot \hat{\boldsymbol{u}}(p) = \sum_{a=1}^{n} \phi^a(\boldsymbol{x})\hat{\boldsymbol{u}}^a(p)\,, \tag{15}$$

where the nodal values $\hat{\boldsymbol{u}}^a(p)$ are fictitious parameters and $\phi^a(\boldsymbol{x})$ is the shape function associated with the node a. The number of nodes n used for the approximation of $\overline{u}_i(\boldsymbol{x},p)$ is determined by the weight function $w^a(\boldsymbol{x})$. A 4^{th} order spline-type weight function is considered in the present work

$$w^a(\boldsymbol{x}) = \begin{cases} 1-6\left(\frac{d^a}{r^a}\right)^2+8\left(\frac{d^a}{r^a}\right)^3-3\left(\frac{d^a}{r^a}\right)^4, & 0 \le d^a \le r^a \\ 0 & d^a \ge r^a \end{cases} \tag{16}$$

where $d^a = \|\boldsymbol{x}-\boldsymbol{x}^a\|$ and r^a is the size of the support domain. It is seen that the C^1-continuity is ensured over the entire domain, therefore the continuity condition of tractions is satisfied. A necessary condition for a well-defined MLS approximation is that the number of nodes lying inside the support domain has to be equal or higher than the order of the polynomial basis [Atluri and Shen (2002)]. In our analyses we have considered $r^a = 4h$, where h is a minimal distance of two neighbouring nodes.

The traction vector $\overline{t}_i(\boldsymbol{x},p)$ at a boundary point $\boldsymbol{x} \in \partial\Omega_s$ is approximated by the same nodal values $\hat{\boldsymbol{u}}^a(p)$ as

$$\overline{\boldsymbol{t}}^h(\boldsymbol{x},p) = \boldsymbol{N}(\boldsymbol{x})\boldsymbol{D}\sum_{a=1}^{n} \boldsymbol{B}^a(\boldsymbol{x})\hat{\boldsymbol{u}}^a(p)\,, \tag{17}$$

where the matrix $\boldsymbol{N}(\boldsymbol{x})$ is related to the unit normal vector $\boldsymbol{n}(\boldsymbol{x})$ on $\partial\Omega_s$ by

$$\boldsymbol{N}(\boldsymbol{x}) = \begin{bmatrix} n_1 & 0 & n_2 \\ 0 & n_2 & n_1 \end{bmatrix},$$

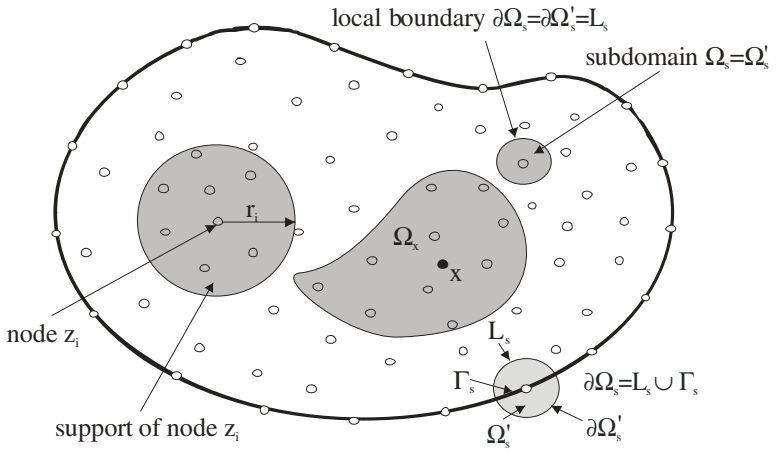

Figure 1 : Global and local boundaries

and the matrix $\boldsymbol{B}^a$ is represented by the gradients of the shape function as

$$\boldsymbol{B}^a = \begin{bmatrix} \phi^a_{,1} & 0 \\ 0 & \phi^a_{,2} \\ \phi^a_{,2} & \phi^a_{,1} \end{bmatrix}.$$

One of the most important properties of the MLS approximation is the continuity of the approximated fields. Continuity is often a desirable property. However, crack analysis requires a modeling of discontinuous displacement fields across the crack-faces. The treatment of the crack displacement discontinuities can be analyzed in several ways in the meshless approximation [Organ et al. (1996); Carpinteri et al. (2003)]. The simplest approach to consider the displacement discontinuity on the crack-faces is the visibility criterion. Accordingly, nodes lying inside the "invisible" domain ABC in Figure 2 are not considered for the evaluation of the shape function (i.e., the weight function is zero) in the MLS. Another approach for the treatment of the displacement discontinuities both in the meshless and in the FEM is based on the introduction of discontinuous enrichment functions [Belytschko et al. (2001)]. Carpinteri et al. (2003) proposed a method where the crack is virtually extended in the direction of the tangent at the crack-tip. All the weight functions whose support domains intersect the real crack are cut along the crack-line (both the real and the virtual), while the weight functions are left unchanged if the support domains intersect only the virtual crack. This method is applied in this paper to analyze a slanted crack.

Obeying the boundary conditions at those nodal points on the global boundary, where displacements are prescribed, and making use of the approximation formula (15), one obtains the discretized form of the displacement boundary conditions given as

$$\sum_{a=1}^{n} \phi^a(\boldsymbol{\zeta})\hat{\boldsymbol{u}}^a(p) = \tilde{\overline{\boldsymbol{u}}}(\boldsymbol{\zeta}, p) \quad \text{for} \quad \boldsymbol{\zeta} \in \Gamma_u. \tag{18}$$

Furthermore, in view of the MLS-approximations (15) and (17) for the unknown fields in the local boundary integral equations (14), we obtain the discretized LIEs

$$\begin{aligned} &\sum_{a=1}^{n} \hat{\boldsymbol{u}}^a(p) \int_{L_s} \boldsymbol{N}(\boldsymbol{x})\boldsymbol{D}(\boldsymbol{x})\boldsymbol{B}^a(\boldsymbol{x}) d\Gamma \\ &+ \sum_{a=1}^{n} \hat{\boldsymbol{u}}^a(p) \int_{\Gamma_{su}} \boldsymbol{N}(\boldsymbol{x})\boldsymbol{D}(\boldsymbol{x})\boldsymbol{B}^a(\boldsymbol{x}) d\Gamma \\ &- p^2 \sum_{a=1}^{n} \hat{\boldsymbol{u}}^a(p) \int_{\Omega_s} \rho(x)\phi^a(\boldsymbol{x}) d\Omega \\ &= -\int_{\Gamma_{st}} \tilde{\overline{\mathbf{t}}}(\boldsymbol{x}, p) d\Gamma - \int_{\Omega_s} \overline{\boldsymbol{F}}(\boldsymbol{x}, p) d\Omega \end{aligned} \tag{19}$$

which are considered on the sub-domains adjacent to interior nodes as well as to the boundary nodes on Γ_{st}.

Collecting the discretized LIEs together with the discretized displacement boundary conditions, we get the complete system of linear algebraic equations for the computation of the nodal unknowns which are the Laplace-transforms of the fictitious parameters $\hat{\boldsymbol{u}}^a(p)$.

The time-dependent values of the transformed variables can be obtained by an inverse transform. There are many inversion methods available for the Laplace-transform.

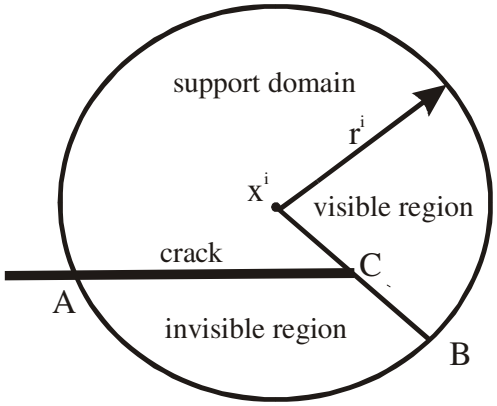

Figure 2 : Visibility criterion for the support domain in the crack-tip vicinity

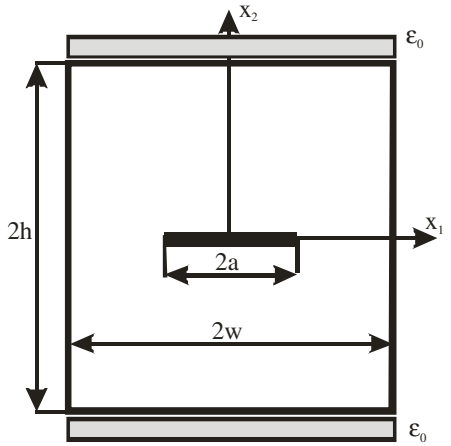

Figure 3 : A finite plate with a center crack parallel to the material gradation

As the Laplace transform inversion is an ill-posed problem, small truncation errors can be greatly magnified in the inversion process and lead to poor numerical results. In the present analysis the Stehfest's algorithm [Stehfest (1970)] is used. An approximate value f_a of the inverse $f(t)$ for a specific time t is given by

$$f_a(t) = \frac{\ln 2}{t} \sum_{i=1}^{N} v_i \overline{f}\left(\frac{\ln 2}{t} i\right), \tag{20}$$

where

$$v_i = (-1)^{N/2+i} \sum_{k=[(i+1)/2]}^{\min(i,N/2)} \frac{k^{N/2}(2k)!}{(N/2-k)!\,k!\,(k-1)!\,(i-k)!\,(2k-i)!}. \tag{21}$$

Numerical experiences show that a truncation number N = 10 with a single precision arithmetic is optimal to obtain accurate numerical results. It means that for each time t, it is needed to solve N boundary value problems for the corresponding Laplace-transform parameters $p = i\ln 2/t$, with $i = 1, 2, ..., N$. If M denotes the number of the time instants in which we are interested to know $f(t)$, the number of the Laplace-transform solutions $\overline{f}(p_j)$ is then $M \times N$.

4 Numerical examples

4.1 A finite plate with a center crack

In the first numerical example a rectangular orthotropic plate with a central crack is analyzed. The plate is considered to be under a fixed-grip loading with a prescribed uniform static deformation ε_0 as shown in Fig. 3. The following geometry is considered: $w = 10$, $a/w = 0.1, 0.2, 0.3$, and $h = w$. Firstly, isotropic material properties with an exponential variation of the Young's modulus parallel to the crack-line are considered

$$E(x) = E_0 \exp(\alpha x_1), \tag{22}$$

with $E = 10^4$, and a constant Poisson's ratio $\nu = 0.3$. Due to symmetry of the problem only a half of the cracked plate is numerically analyzed. A regular node distribution with $61 \times 30 = 1830$ nodes (61 nodes along each line x_2 =const) is used in numerical calculations. The stress intensity factor is computed from the asymptotic expressions for the displacements at the crack-tip, i.e., Eq. (7). In a pure mode-I crack problem, the normal displacement on the crack-face can be written as

$$u_2 = 2\sqrt{\frac{2r}{\pi}} D_{21} K_I, \tag{23}$$

where r is the radial distance of the evaluation point from the crack-tip, and

$$D_{21} = Im\left\{\frac{\mu_2 P_{21} - \mu_1 P_{22}}{\mu_1 - \mu_2}\right\}.$$

The stress intensity factors are normalized as $f_I(\pm a) = K_I(\pm a)/E_0\varepsilon_0\sqrt{\pi a}$. Numerical results are compared with those obtained by Dolbow and Gosz (2002) by the extended finite element method (X-FEM). For an infinite plate with a central crack, numerical solution has been

given by Konda and Erdogan (1994). Then, for the shortest crack, e.g., $a/w = 0.1$, it is possible to make a comparison with the numerical results of Konda and Erdogan (1994). Numerical results for isotropic case and $\alpha = 0.25$ are presented in Tab. 1, which shows a good agreement with that of Dolbow and Gosz (2002).

Next, orthotropic material properties with a constant Poisson's ratio $\nu_{12} = 0.3$ and a constant shear modulus $G_{12} = 6GPa$ are considered for the crack problem analyzed above. Young's moduli are expressed as a function of the parameter $R = E_1/E_2$ with $E_1 = G_{12}(R + 2\nu_{12} + 1)$ and $E_2 = E_1/R$. Two different ratios $R = 0.5$ and 4.5 are considered in our numerical analyses. Also here, Young's moduli E_i have an exponential variation in the x_1-direction

$$E_i(x) = E_{i0}\exp(\alpha x_1)\,. \tag{24}$$

Numerical results for the normalized stress intensity factors $f_I(\pm a) = K_I(\pm a)/\varepsilon_0 E_{20}\sqrt{\pi a}$ are given in Tab. 2. The used gradation exponent α is the same as in the previous isotropic case. One can observe that the orthotropy parameter R has a relatively small influence on the value of the normalized stress intensity factors, at least in the case investigated here.

4.2 A finite plate with an edge crack

In the second numerical example a rectangular plate with an edge crack is analyzed. The following plate and crack geometry is considered: plate-width $w = 1$, crack-length $a/w = 0.5$, and half-length of the plate $h = 4w$ (see Fig.4). The plate is subjected to a uniform stress loading σ in the direction perpendicular to the crack-line. Due to symmetry of the problem, only the upper half of the rectangular plate is discretized. A regular node distribution with 31x30=930 nodes is used. Orthotropic material properties with a constant Poisson's ratio $\nu_{12} = 0.3$ and a constant shear modulus $G_{12} = 6GPa$ are taken here again. Young's moduli are expressed as a function of the parameter $R = E_1/E_2$ with $E_1 = G_{12}(R + 2\nu_{12} + 1)$ and $E_2 = E_1/R$. The Young's modulus E_1 has the same exponential variation in the x_1-direction like in the previous example and the gradient exponent is given by $\alpha = \ln(E_{10}/E_{1w})/w$, with E_{10} and E_{1w} corresponding to the E_1-values at $x_1 = 0$ and $x_1 = w$, respectively. Numerical results for the normalized mode-I stress intensity factor $f_I = K_I/\sigma\sqrt{\pi a}$ are given in Tab. 3. Table 3 shows a good agreement of our numerical results with the FEM results of Kim and Paulino (2002) for isotropic case $R = 1.0$. The percentage error is less than 1.3% and 1.1% for $E_{1w}/E_{10} = 0.2$ and 5.0, respectively.

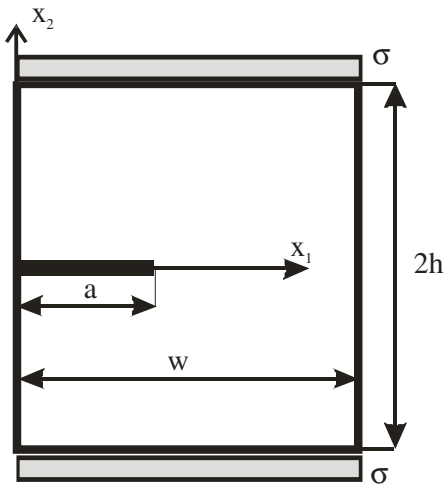

Figure 4 : An edge-cracked orthotropic plate with the material gradation in x_1-direction

The same orthotropic cracked plate under a bending load is analyzed too. The plate is subjected to a linear stress loading $\sigma_{22} = \sigma_b(1 - 2x_1/w)$. Numerical results for the normalized mode-I stress intensity factor $f_I = K_I/\sigma_b\sqrt{\pi a}$ are given in Tab. 4. For an isotropic FGM plate with an edge crack, our results are in good agreement with that of Rao and Rahman (2003) by using a mesh-free method.

In the next example, a rectangular orthotropic and linear elastic FGM plate with an edge crack subjected to an impact loading is analyzed. The plate has the length $2h = 30$, the width $w = 10$, and the crack-length $a/w = 0.4$ (see Fig. 4). At the top and the bottom of the plate, a uniform impact tensile stress $\sigma_{22}(t) = \sigma H(t - 0)$ with the Heaviside step time variation is applied. Orthotropic material properties with a constant Poisson's ratio $\nu_{12} = 0.3$, a constant shear modulus $G_{12} = 0.385 \times 10^4 N/mm^2$, and a mass density $\rho = 10^{-3} kg/mm^3$ are considered. The Young's moduli E_i have the same exponential variations as in the previous static case. Also here a regular node distribution with 930 nodes is used for the discretization.

The dynamic stress intensity factor is normalized by the static value $K_I^{stat} = \sigma\sqrt{\pi a}$ for convenience. The time variations of the mode-I dynamic stress intensity factor are presented in Fig. 5. The used gradient parameter α corresponds to the ratio of Young's moduli $E_{1w}/E_{10} = 5.0$ in the FGM plate. The influence of

Table 1 : Normalized mode-I stress intensity factors in an isotropic FGM plate with a center crack

$\alpha = 0.25$	$a/w = 0.1$		$a/w = 0.2$	$a/w = 0.3$
	[Dolbow & Gosz, 2002]	[MLPG]	[MLPG]	[MLPG]
$f_I(a)$	1.218	1.21	1.460	1.811
$f_I(-a)$	0.838	0.834	0.691	0.572

Table 2 : Normalized stress intensity factors in an orthotropic FGM plate with a center crack

R	$a/w = 0.1$		$a/w = 0.2$		$a/w = 0.3$	
	$f_I(a)$	$f_I(-a)$	$f_I(a)$	$f_I(-a)$	$f_I(a)$	$f_I(-a)$
0.5	1.25	0.853	1.496	0.712	1.902	0.598
4.5	1.19	0.822	1.417	0.669	1.735	0.549

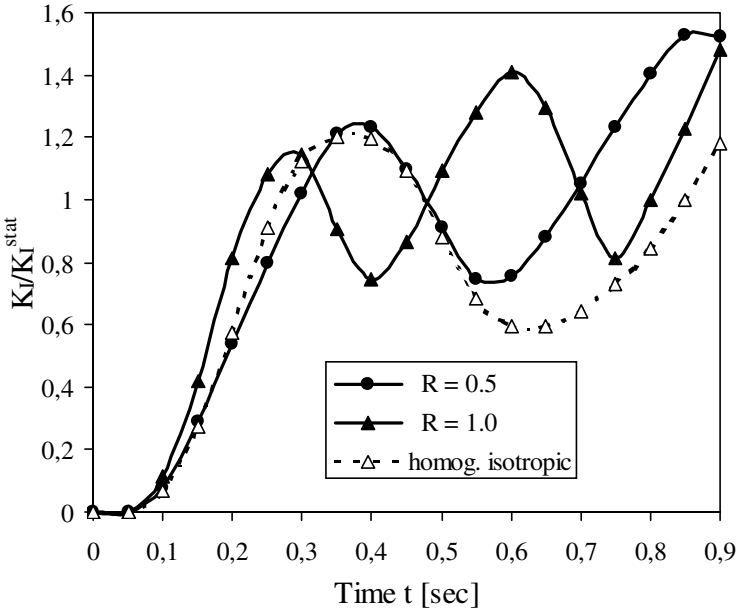

Figure 5 : Normalized mode-I dynamic stress intensity factors for an FGM plate with an edge crack

the material anisotropy, characterized by the parameter $R = E_1/E_2$, on the dynamic stress intensity factor is presented in Fig. 5. Numerical results for the corresponding isotropic case have been obtained by Sladek et al. (2005). If the Young's modulus in the x_1-direction is lower than in the direction perpendicular to the crack line, e.g., R = 0.5, the wave velocity in the x_1-direction is lower too, and the peak values of the normalized mode-I dynamic stress intensity factor are reached at larger time instants than in the isotropic case $R = 1.0$. For $R > 1.0$ the effect of the material anisotropy on the position of the peak $K_I(t)$-values is expected to be opposite.

4.3 A finite plate with a slanted edge crack

The last problem investigated in this paper is a finite plate with a slanted edge crack as depicted in Fig. 6 under a uniform tension with the Heaviside time step variation. For comparison purposes, the geometry of the specimen and the material constants are selected as the same as used in Albuquerque et al. (2004): $h = 44mm$, $w = 32mm$, $c = 6mm$, $a = 22.63mm$ and $\alpha = 45^o$. Plane stress condition is considered. The material is orthotropic with Young's moduli $E_1 = 82.4\,GPa$, $E_2 = 164.8\,GPa$, shear modulus $G_{12} = 29.4\,GPa$, Poisson's ratio $\nu_{12} = 0.4$, and mass density $\rho = 2450\,kg/m^3$. To compare our numerical results with that of Albuquerque et al. (2004), homogeneous or uniform material properties are first as-

Table 3 : Normalized stress intensity factors in an orthotropic FGM plate with an edge crack under tension

E_{1w}/E_{10}	$R=1.0$		$R=0.5$	$R=4.5$
	f_I [Kim & Paulino, 2002]	f_I [MLPG]	f_I [MLPG]	f_I [MLPG]
0.2	3.292	3.25	3.55	3.00
5.0	2.366	2.34	2.56	2.15

Table 4 : Normalized stress intensity factors in an orthotropic FGM plate with an edge crack under bending

E_{1w}/E_{10}	$R=1.0$		$R=0.5$	$R=4.5$
	f_I [Rao& Rahman, 2003]	f_I [MLPG]	f_I [MLPG]	f_I [MLPG]
0.2	1.9322	1.91	2.07	1.75
5.0	1.166	1.154	1.26	1.08

sumed in the analyzed domain. A regular node distribution with $55 \times 50 = 2750$ nodes (55 nodes along each line $x_2 = const$) is used in the numerical calculations. The dynamic stress intensity factor is normalized by $K^{stat} = \sigma\sqrt{\pi a}$ for convenience. Figures 7 and 8 show the time variations of the normalized dynamic stress intensity factors. One can observe a very good agreement of the present and the BEM [Albuquerque et al. (2004)] results. Next, Young's moduli are considered to be continuously varying with Cartesian coordinates. Here, Young's modulus E_1 is assumed to have the same exponential variation in the x_1-direction as in the previous example and the gradient exponent is given by $\alpha = \ln(E_{10}/E_{1w})/w$, with E_{10} and E_{1w} corresponding to the E_1-values at $x_1 = 0$ and $x_1 = w$, respectively. Numerical results for normalized mode-I and mode-II dynamic stress intensity factors are presented in Figs. 9 and 10 for a nonhomogeneity ratio $E_{10}/E_{1w} = 0.5$. Figures 9 and 10 show that the peak values of the normalized dynamic stress intensity factors are reached at larger time instants than in the corresponding homogeneous case. Opposite phenomena is expected for a nonhomogeneity ratio $E_{10}/E_{1w} > 1$.

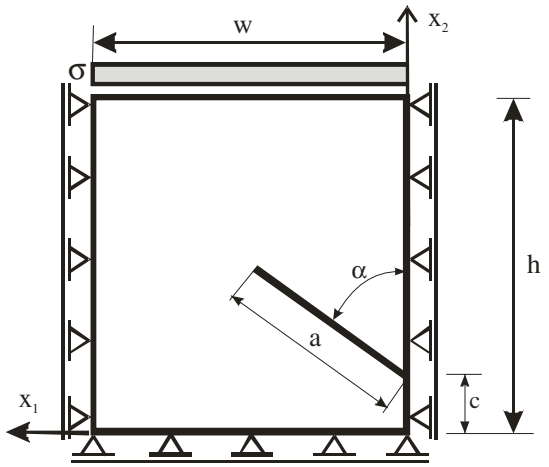

Figure 6 : A finite plate with a slanted edge crack under a uniform tension

5 Conclusions

A local boundary integral equation formulation based on the MLPG in the Laplace-transform domain with a meshless approximation has been successfully implemented to solve 2-d boundary and initial-boundary value problems for static and dynamic crack problems in continuously nonhomogeneous anisotropic and linear elastic solids.

A unit step function is used as the test function in the local symmetric weak-form on the local subdomains. The derived local boundary-domain integral equations are non-singular. The analyzed domain is divided into small overlapping circular sub-domains on which the local boundary integral equations are applied. The proposed method is a truly meshless method, wherein no elements or background cells are involved in either the interpolation or the integration.

The proposed method yields a pure contour-integral method for static crack problems even with nonhomogeneous material properties.

The main difficulty in the application of the classical boundary integral equation formulations for nonhomogeneous anisotroipc and linear elastic solids is the absence of well-established fundamental solutions. This difficulty is overcome by using the present local integral equation method. The computational accuracy of the present method is comparable with that of FEM. However, the adaptability of the present method is expected to be higher than in the conventional FEM, since no mesh generation and remeshing are needed in the present

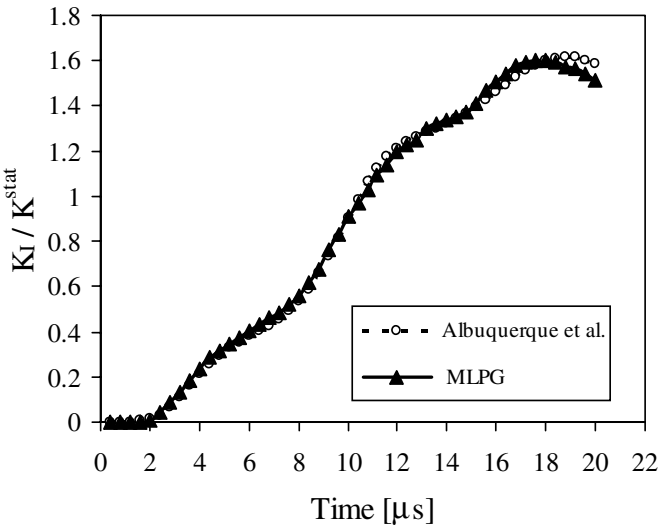

Figure 7 : Normalized mode-I dynamic stress intensity factor for a slanted edge crack in a homogenoeus orthotropic plate

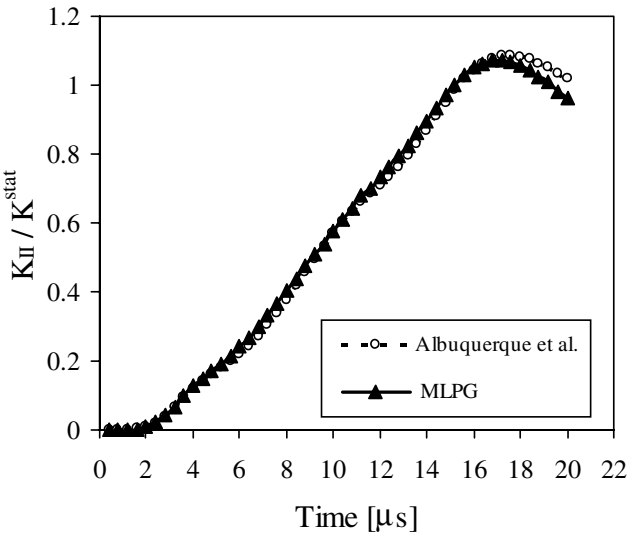

Figure 8 : Normalized mode-II dynamic stress intensity factor for a slanted edge crack in a homogeneous orthotropic plate

method.

Acknowledgement: The authors acknowledge the supports by the Slovak Science and Technology Assistance Agency registered under the project number APVT-51-003702, by the Slovak Grant Agency under the project number VEGA – 2303823, and the project supported jointly by the German Academic Exchange Service (DAAD) and the Ministry of Education of Slovak Republic under the project number D/04/25722.

References

Albuquerque, E.L.; Sollero, P.; Aliabadi, M.H. (2002a): The boundary element method applied to time dependent problems in anisotropic materials. *Int. Journal Solids and Structures*, 39: 1405-1422.

Albuquerque, E.L.; Sollero, P.; Fedelinski, P. (2002b): Boundary element method applied to modal analysis of anisotropic structures, in: *Boundary Element Techniques* (eds. Z. Yao, M.H. Aliabadi), Springer, 65-70.

Albuquerque, E.L.; Sollero, P.; Aliabadi, M.H. (2004): Dual boundary element method for anisotropic dynamic fracture mechanics. *Int. J. Num. Meth. Eng.*, 59: 1187-1205.

Atluri, S. N.; Shen, S. (2002): *The Meshless Local Petrov-Galerkin (MLPG) Method.* Tech Science Press.

Atluri, S.N.; Sladek, J.; Sladek, V.; Zhu, T. (2000): The local boundary integral equation (LBIE) and its meshless implementation for linear elasticity. *Comput. Mech.*, 25: 180-198.

Atluri, S.N.; Han, Z.D.; Shen, S. (2003): Meshless local Petrov-Galerkin (MLPG) approaches for solving the weakly-singular traction & displacement boundary integral equations. *CMES: Computer Modeling in Engineering & Sciences*, 4: 507-516.

Atluri, S.N. (2004): *The Meshless Local Petrov-Galerkin Method for Domain & BIE Discretizations.* Tech Science Press.

Belytschko, T.; Lu, Y.; Gu, L. (1994): Element free Galerkin methods. *Int. J. Num. Meth. Engn.*, 37: 229-256.

Belytschko, T.; Krogauz, Y.; Organ, D.; Fleming, M.; Krysl, P. (1996): Meshless methods; an overview and recent developments. *Comp. Meth. Appl. Mech. Engn.*, 139: 3-47.

Belytschko, T.; Moes, N.; Usi, S.; Parimi, C. (2001): Arbitrary discontinuities in finite elements. Int. J. Num. Meth. Eng., 50: 993-1013.

Bowie, O.L.; Freeze, C.E. (1972): Central crack in plane orthotropic rectangular sheet. *International Jour-*

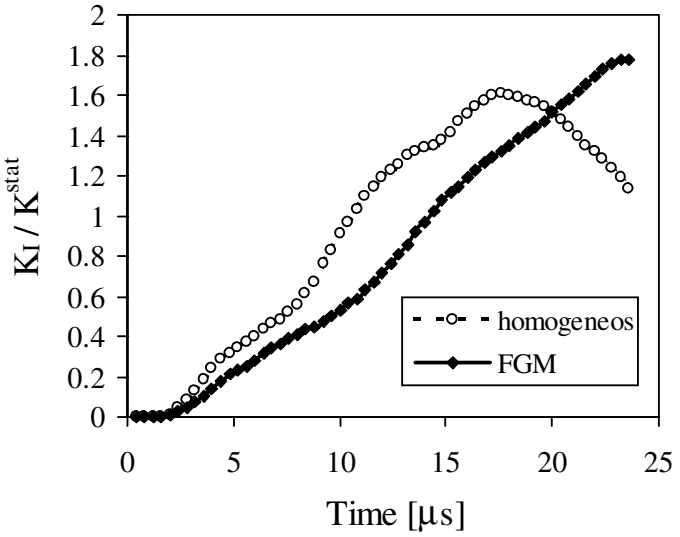

Figure 9 : Normalized mode-I dynamic stress intensity factor for a slanted edge crack in an FGM plate

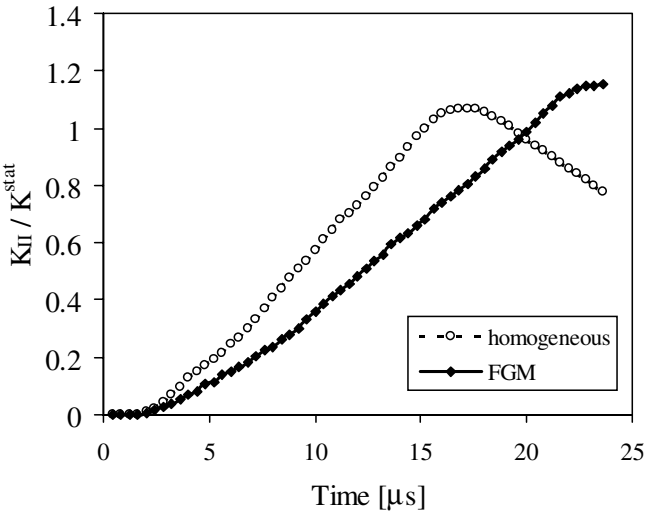

Figure 10 : Normalized mode-II dynamic stress intensity factor for a slanted edge crack in an FGM plate

nal of Fracture, 8: 49-58.

Carpinteri, A.; Ferro, G.; Ventura, G. (2003): The partition of unity quadrature in element-free crack modeling. *Computers & Structures*, 81: 1783-1794.

Ding, H.; Liang, J.; Chen, B. (1997): The unit point force solution for both isotropic and transversaly isotropic media. *Communications in Numerical Methods in Engineering*, 13: 95-102.

Dolbow, J.E.; Gosz, M. (2002): On the computation of mixed-mode stress intensity factors in functionally graded materials. *Int. J. Solids and Structures,* 39: 2557-2574.

Erdogan, F. (1995): Fracture mechanics of functionally graded materials. *Compos. Eng.,* 5: 753-770.

Eshelby, J.D; Read, W.T.; Shockley, W. (1953): Anisotropic elasticity with applications to dislocations. *Acta Metallurgica*, 1: 251-259.

Gu, P.; Asaro, R.J. (1997): Cracks in functionally graded materials. *Int. J. Solids and Structures,* 34: 1-17.

Kim, J.H.; Paulino, G.H. (2002): Finite element evaluation of mixed mode stress intensity factors in functionally graded materials. *Int. J. Num. Meth. Engn.,* 53: 1903-1935.

Kim, J.H.; Paulino, G.H. (2003a): T-stress, mixed mode stress intensity factors, and crack initiation angles in functionally graded materials: A unified approach using the interaction integral method. *Comp. Meth. Appl. Mech. Engn.,* 192: 1463-1494.

Kim, J.H.; Paulino, G.H. (2003b): The interaction integral for fracture of orthotropic functionally graded materials: Evaluation of stress intensity factors. *Int. J. Solids and Structures,* 40: 3967-4001.

Kim, J.H.; Paulino, G.H. (2004): T-stress in orthotropic functionally graded materials: Lekhnitskii and Stroh formalisms. *Int. J. Fracture,* 126: 345-384.

Kögl, M.; Gaul, L. (2000): A 3-D boundary element method for dynamic analysis of anisotropic elastic solids. *CMES: Computer Modeling in Engn. & Sciences*, 1: 27-43.

Lekhnitskii, S.G. (1963): *Theory of Elasticity of an Anisotropic Body.* Holden Day.

Konda, N.; Erdogan, F. (1994): The mixed mode crack problem in a nonhomogeneous elastic medium. *Eng. Fracture Mech.,* 47: 533-545.

Mikhailov, S.E. (2002): Localized boundary-domain integral formulations for problems with variable coefficients. *Eng. Analysis with Boundary Elements*, 26: 681-690.

Murakami, Y. (1987): *Stress Intensity Factor Handbook*, Pergamon Press.

Organ, D.; Fleming, M.; Terry, T.; Belytschko, T. (1996): Continuous meshless approximations for convex bodies by diffraction and trancaparency. *Comput. Mech*., 18: 1-11.

Ozturk, M.; Erdogan, F. (1997): Mode I crack problem in an inhomogeneous orthotropic medium. *Int. J. Engn. Sci.,* 35: 869-883.

Ozturk, M.; Erdogan, F. (1999): The mixed mode crack problem in an inhomogeneous orthotropic medium. *Int. J. Fracture*, 98: 243-261.

Paulino, G.H.; Jin, Z.H.; Dodds, R.H. (2003): *Failure of functionally graded materials.* In: Karihaloo B, Knauss WG, editors, *Comprehensive Structural Integrity*, Volume 2, Elsevier Science, 607-644.

Rao, B.N.; Rahman, S. (2003): Mesh-free analysis of cracks in isotropic functionally graded materials. *Eng. Fracture Mechanics,* 70: 1-27.

Schclar, S.N. (1994): *Anisotropic Analysis Using Boundary Elements.* Computational Mechanics Publications.

Sih, G.C.; Paris, P.C.; Irwin, G.R. (1965): On cracks in rectilinearly anisotropic bodies. *Int. J. Fracture Mechanics,* 1: 189-203

Sladek, V.; Sladek, J. (1983): Transient elastodynamic three-dimensional problems in cracked bodies. *Applied Mathematical Modelling*, 8: 2-10.

Sladek, V.; Sladek, J.; Markechova, I. (1993): An advanced boundary element method for elasticity problems in nonhomogeneous media. *Acta Mechanica*, 97: 71-90.

Sladek, J.; Sladek, V.; Atluri, S.N. (2000): Local boundary integral equation (LBIE) method for solving problems of elasticity with nonhomogeneous material properties. *Computational Mechanics,* 24: 456-462.

Sladek, J.; Sladek, V.; Van Keer, R. (2003a): Meshless local boundary integral equation method for 2D elastodynamic problems. *Int. J. Num. Meth. Eng*., 57: 235-249

Sladek, J.; Sladek, V.; Zhang, Ch. (2003b): Application of meshless local Petrov-Galerkin (MLPG) method to elastodynamic problems in continuously nonhomogeneous solids. *CMES: Computer Modeling in Eng. & Sciences*, 4: 637-648.

Sladek, J.; Sladek, V.; Atluri, S.N. (2004): Meshless local Petrov-Galerkin method in anisotropic elasticity. *CMES: Computer Modeling in Engn. & Sciences*, 6: 477-489.

Sladek, J.; Sladek, V.; Zhang, Ch. (2005)**:** An advanced numerical method for computing elastodynamic fracture parameters in functionally graded materials. *Computational Materials Science,* 32: 532-543.

Sollero, P.; Aliabadi M.H. (1993): Fracture mechanics analysis of anisotropic plates by the boundary element method. *International Journal of Fracture,* 64: 269-284.

Stehfest, H. (1970): Algorithm 368: numerical inversion of Laplace transform. *Comm. Assoc. Comput. Mach*., 13: 47-49.

Suresh, S.; Mortensen, A. (1998): *Fundamentals of Functionally Graded Materials*. Institute of Materials, London.

Wang, C.Y.; Achenbach, J.D. (1996): Two dimensional time domain BEM for scattering of elastic waves in solids of general anisotropy. *International Journal of Solids and Structures*, 33: 3843-3864.